

Interaction of molecular nitrogen with free-electron laser radiation

H. I. B. Banks^a, D. A. Little^a, J. Tennyson^a and A. Emmanouilidou^a

We compute molecular continuum orbitals in the single center expansion scheme. We then employ these orbitals to obtain molecular Auger rates and single-photon ionization cross sections to study the interaction of N₂ with free-electron laser (FEL) pulses. The nuclei are kept fixed. We formulate rate equations for the energetically allowed molecular and atomic transitions and we account for dissociation through additional terms in the rate equations. Solving these equations for different parameters of the FEL pulse, allows us to identify the most efficient parameters of the FEL pulse for obtaining the highest contribution of double core hole (DCH) states in the final atomic ion fragments. Finally we identify the contribution of DCH states in the electron spectra and show that the DCH state contribution is more easily identified in the photo-ionization rather than the Auger transitions.

1 Introduction

The development of x-ray free-electron lasers (FELs)¹ has introduced new tools for imaging and exploring novel states of atoms and molecules.^{2,3} Potential applications of FELs range from imaging biomolecules⁴⁻⁶ to accurate modeling of laboratory and astrophysical plasmas. FEL driven processes in atoms and molecules include single-photon ionization and Auger processes. Sequential single-photon ionization processes occurring on a time scale that is faster than Auger decays lead to the formation of inner-shell holes in atoms and molecules. In an Auger process a valence electron drops in to fill a core hole; the energy released allows another valence electron to escape to the continuum. The formation of double core hole (DCH) states in molecules is of particular interest for chemical analysis^{7,8}. The energy required to remove a core electron depends upon the chemical environment of the site the electron is removed from rendering DCHs a sensitive spectroscopic tool for chemical analysis.

To understand the formation and detection of single core hole (SCH) and DCH states in molecules, one must explore the interplay of Auger and photo-ionization processes. There has been a significant amount of work on calculating the Auger rates and photo-ionization cross sections in atoms.⁹⁻¹⁴ The work on computing these rates for molecules is significantly less. The reason is that molecules do not have spherical symmetry and thus computing the molecular continuum orbital of the escaping electron is a complex task. This in turn hinders the computation of the Auger rates and the single-photon ionization cross sections in molecules.

Previous molecular studies with FEL radiation include models where the molecule is treated as a combination of atoms. Then, in these models, the Auger rates and the photo-ionization cross sections are computed for atomic transitions.^{15,16} These atomic rates are then used to setup rate equations to describe molecular interactions with FEL radiation. In some instances dissociation is accounted for through additional terms in the rate equations.^{15,16} For high photon energy FEL pulses interacting with N₂, these models have been used to compute the yields of the final atomic ion

fragments as well as the contribution of the DCH molecular states in the yields of the final atomic ions.^{15,16} Very recently, new methods have been developed to describe molecular states with multiple holes and to compute molecular transitions following interaction with FEL radiation.^{17,18} These new methods have been employed to compute the yields of the final molecular ion states as well as the contribution of SCH and DCH states in water for fixed nuclei.¹⁹ The calculations in these studies were performed with atomic continuum orbitals rather than molecular ones. The use of atomic continuum orbitals is a good approximation when these models are employed to study molecular interactions with high photon energy FEL pulses.

N₂ interacting with FEL pulses has been the subject of many experimental studies.²⁰⁻²² In these studies the yields of the final atomic ion states and the formation of molecular DCHs are investigated. In this work, we study the interaction of the N₂ diatomic molecule with FEL radiation. To do so, we assume that the nuclei are fixed, an assumption also made in previous studies.^{15,16,19} Very importantly, we compute the molecular continuum orbitals. We then employ these orbitals to compute the Auger rates and the single-photon ionization cross sections for all molecular transitions that are energetically accessible. This way our studies are not restricted to high photon FEL pulses. Specifically, we investigate the interaction of a 525 eV and a 1100 eV FEL pulse with N₂. These photon energies are sufficient to create three inner-shell holes through sequential single-photon absorptions and multiple valence holes in the ground state of N₂. Moreover, as we show in the section concerning electron spectra, for a 525 eV FEL pulse some of the electrons ionize with very small energies. These small energies render necessary the use of molecular continuum orbitals, as is done in the current work. We compute the Auger and the single-photon ionization processes for the molecular transitions allowed, thus improving over previous studies that consider only atomic transitions.¹⁶ We then set up rate equations for the allowed molecular and atomic transitions and account for dissociation through additional terms in the rate equations. We also investigate the dependence of the final molecular and atomic ion fragments on the intensity and pulse duration of the FEL pulse. Moreover, we compute all energetically accessible pathways and

^a Department of Physics and Astronomy, University College London, Gower Street, London WC1E 6BT, United Kingdom. E-mail: a.emmanouilidou@ucl.ac.uk

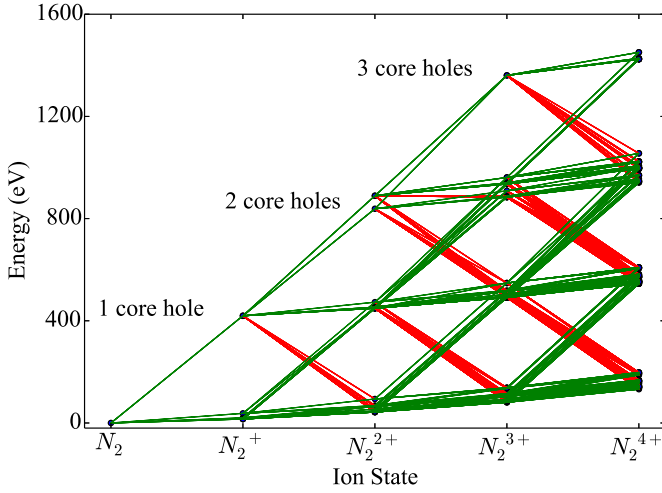


Fig. 1 Ionization pathways between different electronic configurations of N_2 up to N_2^{4+} , accessible with sequential single-photon ($\hbar\omega = 525\text{eV}$) absorptions and Auger decays. The green and red lines indicate photo-ionization and Auger transitions, respectively

can thus determine the contribution of the DCH molecular states in the final atomic ion states as well as in the electron spectra. Finally, we investigate whether photo-ionization or Auger transitions in the electron spectra are more effective in detecting the formation of DCH molecular states.

2 Ion Yields and Pathways

We study the response of N_2 to FEL pulses of photon energies 525 eV and 1100 eV. We do so by formulating and solving a set of rate equations for the time dependent population of the ion states.

2.1 Rate Equations

We construct rate equations for each energetically accessible state of molecular nitrogen. Each molecular state is denoted by its electronic configuration ($1\sigma_g^a, 1\sigma_u^b, 2\sigma_g^c, 2\sigma_u^d, 1\pi_{ux}^e, 1\pi_{uy}^f, 3\sigma_g^g$) with a, b, c, d, e, f, g the number of electrons occupying a molecular orbital. Each occupation number is equal to 0, 1 or 2. 2 corresponds to the maximum occupancy of a molecular orbital of two electrons with spin up and down. Atomic units are used in this work, unless otherwise stated. In Fig. 1, accounting for states up to N_2^{4+} , we illustrate the photo-ionization and Auger transitions between molecular states that are accessible due to the interaction of N_2 with a 525 eV laser pulse. To create a core hole, a minimum photon energy of 420 eV is required. The transitions in Fig. 1 were calculated for the ground state equilibrium distance of the nuclei for N_2 . This was done by employing Molpro²³ and performing a Hartree Fock calculation using correlation-consistent polarized triple-zeta (cc-pVTZ) basis set.

We assume that the nuclei are fixed at the equilibrium distance of N_2 of 2.08 a.u.. To model the fragmentation of N_2 that leads to the formation of atomic ions, we include in the rate equations terms accounting for dissociation. Specifically, we assume that instantaneous dissociation, i.e. a very large dissociation rate, takes

place from the N_2^{4+} and N_2^{3+} molecular states with no core holes. Dissociation of N_2^{3+} and N_2^{4+} leads to $N^+ + N^{2+}$ and $N^{2+} + N^{2+}$, respectively. We further assume that all N_2^{2+} molecular states dissociate with a lifetime of 100 fs.²⁴ N_2^{2+} dissociation leads to $N^+ + N^+$ and $N + N^{2+}$ with probabilities 74% and 26%,²⁴ respectively. The above dissociation processes are similar to the dissociation processes taken into account in ref. 16. In the rate equations fluorescence is not accounted for since the corresponding rates are much smaller compared to Auger and single-photon processes.²⁵ In the rate equations we also account for the states of atomic nitrogen that are accessible through molecular fragmentation and through single-photon ionization and Auger processes occurring in the atomic ion states. Each atomic state is denoted by ($1s^a, 2s^b, 2p^c$) with a, b and c the occupation numbers of the atomic orbitals.

The rate equations describing the population $\mathcal{I}_j(t)$ of a molecular ion state j take the form

$$\frac{d}{dt}\mathcal{I}_j(t) = \sum_i (\sigma_{i \rightarrow j} J(t) + \Gamma_{i \rightarrow j}) \mathcal{I}_i(t) \quad (1)$$

$$- \sum_k (\sigma_{j \rightarrow k} J(t) + \Gamma_{j \rightarrow k}) \mathcal{I}_j(t) - \sum_n \kappa_{j \rightarrow n,p} \mathcal{I}_j(t),$$

$$\frac{d}{dt}\mathcal{A}_{i \rightarrow j} = \Gamma_{i \rightarrow j} \mathcal{I}_i(t),$$

$$\frac{d}{dt}\mathcal{P}_{i \rightarrow j} = \sigma_{i \rightarrow j} J(t) \mathcal{I}_i(t).$$

$\sigma_{i \rightarrow j}$ and $\Gamma_{i \rightarrow j}$ are the molecular single-photon absorption cross section and Auger decay rate, respectively, from the initial molecular state i to the final molecular state j . $J(t)$ is the photon flux at time t . The temporal form of the FEL flux is modeled with a Gaussian function given by²⁶

$$J(t) = 1.554 \times 10^{-16} \frac{I_0 [\text{W cm}^{-2}]}{\hbar\omega [\text{eV}]} \exp \left\{ -4 \ln 2 \left(\frac{t}{\tau_X} \right)^2 \right\} \quad (2)$$

with τ_X the full width at half maximum (FWHM) and I_0 the peak intensity. The molecular states i, j and k have charges $q-1, q$ and $q+1$, respectively. $\kappa_{j \rightarrow n,p}$ denotes the dissociation rate from the initial molecular state j with charge q to the final atomic states n and p . The atomic states n and p have total charge equal to q . For the dissociation cases currently considered, for each atomic final fragment n there is only one atomic final fragment p . The first term in eqn (1) accounts for the formation of the molecular state j through the single-photon ionization and Auger decay of the molecular state i . The second term in eqn (1) accounts for the depletion of the molecular state j by transitioning to a molecular state k through single-photon ionization and Auger decay. The third term accounts for the depopulation of the molecular state j through dissociation to the atomic states n and p . These rate equations, eqn (1), are used to calculate the molecular ion yields. In addition, in eqn (1), we solve for the Auger $\mathcal{A}_{i \rightarrow j}$ and the photo-ionization $\mathcal{P}_{i \rightarrow j}$ yield from an initial molecular state i with charge $q-1$ to a final molecular state j with charge q . These yields provide the probability for observing an electron with energy corresponding to the molecular transition $i \rightarrow j$. We use these yields to de-

scribe the molecular transitions in the electron spectra produced by the interaction of N₂ with an FEL pulse. The electron spectra are presented later in the paper.

The rate equations describing the populations of an atomic state n take the form

$$\begin{aligned} \frac{d}{dt}\mathcal{I}_n(t) = & \sum_m (\sigma_{m \rightarrow n} J(t) + \Gamma_{m \rightarrow n}) \mathcal{I}_m(t) \\ & - \sum_o (\sigma_{n \rightarrow o} J(t) + \Gamma_{n \rightarrow o}) \mathcal{I}_n(t) + \sum_j \frac{\kappa_{j \rightarrow n, p}}{2 - \delta_{n, p}} \mathcal{I}_j(t), \end{aligned} \quad (3)$$

$$\frac{d}{dt}\mathcal{A}_{m \rightarrow n} = \Gamma_{m \rightarrow n} \mathcal{I}_m(t),$$

$$\frac{d}{dt}\mathcal{P}_{m \rightarrow n} = \sigma_{m \rightarrow n} J(t) \mathcal{I}_m(t),$$

where the indices n, m and o refer to atomic states with charges, q, q-1 and q+1, respectively, while j refers to molecular states. The first term in eqn (3) accounts for the formation of the atomic state n through the single-photon ionization and Auger decay of the atomic state m. The second term in eqn (3) accounts for the depletion of the atomic state n by transitioning to an atomic state o through single-photon ionization and Auger decay. The third term in eqn (3) accounts for the population of state n as a result of dissociative transitions from a molecular state j. The factor $\frac{1}{2 - \delta_{n, p}}$ conserves the population transfer from the molecular state j. Namely, if the molecular state results in the same two atomic fragments the factor is equal to 1. If fragmentation results in two different atomic fragments the factor is equal to $\frac{1}{2}$, since a rate equation is formulated for each atomic fragment separately. As in the molecular rate equations, in eqn (3), we solve for the Auger $\mathcal{A}_{m \rightarrow n}$ and the photoionization $\mathcal{P}_{m \rightarrow n}$ yields from an initial atomic state i with charge q-1 to a final atomic state j with charge q. These yields provide the probability for observing an electron with energy corresponding to the atomic transition $m \rightarrow n$. We use these yields to describe the atomic transitions in the electron spectra produced by the interaction of N₂ with an FEL pulse. We note that eqn (1) and eqn (3) are solved simultaneously. We obtain the molecular and atomic ion yields long after the end of the laser pulse.

It is also of interest to compute the population transfer through a specific pathway $i \rightarrow j \rightarrow k$ where the initial state is i and the final one that is k is reached through the state j. The three types

of relevant rate equations for computing the pathway populations are given by eqns (4-6)

$$\begin{aligned} \frac{d}{dt}\mathcal{I}_{i \rightarrow j \rightarrow k}(t) = & (\sigma_{j \rightarrow k} J(t) + \Gamma_{j \rightarrow k}) \mathcal{I}_{i \rightarrow j}(t) \\ & - \sum_l (\sigma_{k \rightarrow l} J(t) + \Gamma_{k \rightarrow l}) \mathcal{I}_{i \rightarrow j \rightarrow k}(t) - \sum_n \kappa_{k \rightarrow n, p} \mathcal{I}_{i \rightarrow j \rightarrow k}(t), \end{aligned} \quad (4)$$

$$\begin{aligned} \frac{d}{dt}\mathcal{I}_{i \rightarrow j \rightarrow n}(t) = & \frac{\kappa_{j \rightarrow n, p}}{2 - \delta_{n, p}} \mathcal{I}_{i \rightarrow j}(t) \\ & - \sum_o (\sigma_{n \rightarrow o} J(t) + \Gamma_{n \rightarrow o}) \mathcal{I}_{i \rightarrow j \rightarrow n}(t), \end{aligned} \quad (5)$$

$$\begin{aligned} \frac{d}{dt}\mathcal{I}_{i \rightarrow m \rightarrow n}(t) = & (\sigma_{m \rightarrow n} J(t) + \Gamma_{m \rightarrow n}) \mathcal{I}_{i \rightarrow m}(t) \\ & - \sum_o (\sigma_{n \rightarrow o} J(t) + \Gamma_{n \rightarrow o}) \mathcal{I}_{i \rightarrow m \rightarrow n}(t). \end{aligned} \quad (6)$$

The indices i, j, k and l refer to molecular states whereas the indices m, n and o refer to atomic states. Eqn (4) computes molecular pathway populations, eqn (5) computes pathway populations where the final state is an atomic one, but the previous states were molecular. Pathway populations where the final and the previous states are atomic ones are computed using eqn (6). Solving eqns (4-6), allows us to register all energetically-allowed pathways. Each pathway starts from the ground state of N₂ and ends at an accessible atomic or molecular ion state. Obtaining the pathway populations allows to determine the percentage of final ion states that were formed through pathways involving a molecular states with only a single or a double core hole. These results are presented later in the paper.

2.2 Electron Continuum molecular orbitals

An advantage of the rate equations formulated in the previous section is that we compute the single-photon ionization cross sections and the Auger rates using the continuum wave functions of the molecular orbitals. We compute these continuum molecular orbitals by following the formulation in ref. 27. In what follows, we briefly outline the steps we follow to compute the continuum molecular orbitals. The first step in the derivation involves the Hartree-Fock equations²⁸ given by

$$\underbrace{-\frac{1}{2}\nabla^2\phi_\varepsilon(\mathbf{r})}_{\text{Kinetic energy}} + \underbrace{\sum_n^{\text{nuc.}} \frac{-Z_n}{|\mathbf{r}-\mathbf{R}_n|}\phi_\varepsilon(\mathbf{r})}_{\text{Electron-nuclei}} + \underbrace{\sum_i^{\text{orb.}} a_i \int d\mathbf{r}' \frac{\phi_i^*(\mathbf{r}')\phi_i(\mathbf{r}')}{|\mathbf{r}-\mathbf{r}'|}\phi_\varepsilon(\mathbf{r})}_{\text{Direct interaction}} - \underbrace{\sum_i^{\text{orb.}} b_i \int d\mathbf{r}' \frac{\phi_i^*(\mathbf{r}')\phi_\varepsilon(\mathbf{r}')}{|\mathbf{r}-\mathbf{r}'|}\phi_i(\mathbf{r})}_{\text{Exchange interaction}} = \varepsilon\phi_\varepsilon(\mathbf{r}). \quad (7)$$

The index ε denotes a continuum molecular orbital with $\varepsilon > 0$ the energy of the ionizing electron. The index i denotes bound molecular orbitals, where a_i and b_i are coefficients associated with the orbital i. These coefficients are derived in Appendix A. \mathbf{R}_n denotes the position of nucleus n. The electron-nuclei term is the Coulomb

interaction of the continuum electron with each one of the nuclei. The direct and exchange terms arise from the Coulomb interaction of the continuum electron with the bound electrons. To simplify the numerical integrations involved in eqn (7), the bound and continuum orbital wave functions are expressed using the single-

centre expansion (SCE).²⁷ This approximation allows for the angular part of the integrations in eqn (7) to be obtained analytically. According to the SCE the wave function of the molecular orbital i is expressed as

$$\phi_i(\mathbf{r}) = \sum_{lm} \frac{P_{lm}^i(\mathbf{r}) Y_{lm}(\theta, \phi)}{r}, \quad (8)$$

with $\mathbf{r} = (r, \theta, \phi)$ denoting the position of the electron. For continuum orbitals, i is replaced by the energy of the ionizing electron ε . Y_{lm} is a spherical harmonic with quantum numbers l and m . $P_{lm}^i(\mathbf{r})$ are single centre expansion coefficients for the orbital i . Substituting eqn (8) in eqn (7) and then multiplying by Y_{lm}^* and integrating over the angular part results in

$$\sum_{l'm'} \left[\left(-\frac{d^2}{dr^2} + \frac{l(l+1)}{r^2} - 2\varepsilon \right) \delta_{l'l'} \delta_{mm'} + 2V_{lm,l'm'}^{ne}(r) + 2J_{lm,l'm'}^{ce}(r) \right] P_{l'm'}^\varepsilon(r) + 2X_{lm}[\bar{P}^\varepsilon](r) = 0. \quad (9)$$

$V_{lm,l'm'}^{ne}(r)$ is the electron-nuclei interaction, $J_{lm,l'm'}^{ce}(r)$ is the direct interaction term, and $X_{lm}[\bar{P}^\varepsilon](r)$ is the exchange interaction term. In eqn (9), we are solving for $P_{l'm'}^\varepsilon(r)$, which are the coefficients in the SCE of the continuum wavefunction. \bar{P}^ε is the vector form of $P_{l'm'}^\varepsilon(r)$. The electron-nuclei interaction $V_{lm,l'm'}^{ne}(r)$ is given by

$$V_{lm,l'm'}^{ne}(r) = \sum_n^{nuc.} -Z_n (-1)^m \sqrt{(2l+1)(2l'+1)} \times \sum_{kq} \begin{pmatrix} 1 & k & l' \\ 0 & 0 & 0 \end{pmatrix} \begin{pmatrix} 1 & k & l' \\ -m & q & m' \end{pmatrix} \sqrt{\frac{4\pi}{2k+1}} Y_{kq}^*(\theta_n, \phi_n) \frac{r_{<}^k}{r_{>}^{k+1}}, \quad (10)$$

with the angular integration expressed in terms of Wigner 3j-symbols;²⁹ $r_{<} = \min(r, R_n)$ and $r_{>} = \max(r, R_n)$. The direct interaction $J_{lm,l'm'}(r)$ is given by

$$J_{lm,l'm'}(r) = \sum_i a_i \sum_{l_2 m_2, l_3 m_3, kq} \sqrt{(2l+1)(2l'+1)(2l_2+1)(2l_3+1)} \times \begin{pmatrix} l_2 & k & l_3 \\ 0 & 0 & 0 \end{pmatrix} \begin{pmatrix} l_2 & k & l_3 \\ -m_2 & q & m_3 \end{pmatrix} \begin{pmatrix} l' & k & l \\ 0 & 0 & 0 \end{pmatrix} \begin{pmatrix} l' & k & l \\ -m' & q & m \end{pmatrix} \times (-1)^{m_2+m'} \int_0^\infty \frac{r_{<}^k}{r_{>}^{k+1}} P_{l_2 m_2}^{i*}(r') P_{l_3 m_3}^i(r') dr', \quad (11)$$

where $r_{<} = \min(r, r')$ and $r_{>} = \max(r, r')$ and, l_2, m_2 and l_3, m_3 refer to the orbital i . The exchange interaction can be cast as a functional of the SCE coefficients of the continuum electron orbital as

follows

$$X_{lm}[\bar{P}^\varepsilon](r) = \sum_{l'm'}^{orb.} \sum_i b_i \sum_{l_2 m_2, l_3 m_3, kq} \sqrt{(2l+1)(2l'+1)(2l_2+1)(2l_3+1)} \times \begin{pmatrix} l_2 & k & l' \\ 0 & 0 & 0 \end{pmatrix} \begin{pmatrix} l_2 & k & l' \\ -m_2 & q & m' \end{pmatrix} \begin{pmatrix} l_3 & k & l \\ 0 & 0 & 0 \end{pmatrix} \begin{pmatrix} l_3 & k & l \\ -m_3 & q & m \end{pmatrix} \times (-1)^{m_2+m_3} \int_0^\infty \frac{r_{<}^k}{r_{>}^{k+1}} P_{l_2 m_2}^{i*}(r') P_{l' m'}^\varepsilon(r') dr' P_{l_3 m_3}^i(r). \quad (12)$$

For numerical efficiency, $P_{l'm'}^\varepsilon(r)$ are obtained solving eqn (9) with the non-iterative method described in ref. 27. Diatomic molecules have rotational symmetry around the molecular axis and thus m is a good quantum number. Therefore, m_2 and m_3 are equal and have a fixed value for a bound orbital i . In addition, m and m' are equal and have a fixed value determined by the symmetry of the continuum orbital. For the N_2 diatomic molecule, we find that convergence of the continuum orbital is achieved when considering l up to 19 for the single center expansion. As a result, for each energy ε , eqn (9) has at the most 19 degenerate solutions.

2.3 Photo-ionisation Cross-sections

The photo-ionisation cross-section³⁰ for an electron transitioning from an initial molecular orbital ϕ_i to a final continuum molecular orbital ϕ_ε is given by

$$\sigma_{i \rightarrow \varepsilon} = \frac{4}{3} \alpha \pi^2 \omega N_i \sum_{M=-1,0,1} |D_{i\varepsilon}^M|^2, \quad (13)$$

where α is the fine structure constant, N_i is the occupation number of the initial molecular orbital i , ω is the photon energy, and M is the polarization of the photon. In the length gauge, the matrix element $D_{i\varepsilon}^M$ is given by

$$D_{i\varepsilon}^M = \int \phi_i(\mathbf{r}) \phi_\varepsilon(\mathbf{r}) \sqrt{\frac{4\pi}{3}} r Y_{1M}(\theta, \phi) d\mathbf{r}. \quad (14)$$

In the single centre expansion formalism eqn (14) takes the form

$$D_{i\varepsilon}^M = \sqrt{\frac{4\pi}{3}} \sum_{lm, l'm'} \int_0^\infty dr P_{lm}^{i*}(r) r P_{l'm'}^\varepsilon(r) \int d\Omega Y_{lm}^*(\theta, \phi) Y_{l'm'}(\theta, \phi) Y_{1M}(\theta, \phi) \quad (15)$$

$$= \sum_{lm, l'm'} (-1)^m \sqrt{(2l+1)(2l'+1)} \begin{pmatrix} 1 & l' & 1 \\ 0 & 0 & 0 \end{pmatrix} \begin{pmatrix} 1 & l' & 1 \\ -m & m' & M \end{pmatrix} \int_0^\infty dr P_{lm}^{i*}(r) r P_{l'm'}^\varepsilon(r).$$

E_{photon} (eV)	$2\sigma_g \rightarrow \varepsilon\sigma_u$		$2\sigma_g \rightarrow \varepsilon\pi_u$	
	Ref. 31	This Work	Ref. 31	This Work
40	0.035	0.038	0.073	0.20
45	0.58	0.55	0.22	0.38
50	2.6	2.5	0.41	0.52
55	1.9	2.0	0.59	0.63
60	1.1	1.2	0.71	0.69
65	0.74	0.80	0.75	0.73
70	0.54	0.58	0.74	0.73
75	0.40	0.44	0.70	0.72
80	0.31	0.33	0.65	0.69

Table 1 Photo-ionization cross-sections for N_2 transitions: columns 3 and 5 correspond to our results and columns 2 and 4 correspond to previous calculations³¹

In Table 1, for certain transitions in N_2 , we compare with past calculations³¹ the photo-ionization cross sections we compute using eqn (15). Very good agreement is obtained.

2.4 Auger Rates

In general, the Auger rate is given by³²

$$\Gamma = \overline{\sum} 2\pi |\mathcal{M}|^2 \equiv \overline{\sum} 2\pi |\langle \Psi_{\text{fin}} | H_I | \Psi_{\text{init}} \rangle|^2, \quad (16)$$

where $\overline{\sum}$ denotes a summation over the final states and an average over the initial states. $|\Psi\rangle$ is the wavefunction of all electrons in the molecular state. In the Hartree-Fock approximation, $|\Psi\rangle$ is given by a Slater determinant of one-electron spin-orbital wavefunctions. The Auger transition is treated as a two-electron process and therefore the relevant part of H_I is the electron-electron Coulomb interaction term. In the second quantization formalism,^{33,34} this Hamiltonian term is given by

$$H_I^{\text{ee}} = \frac{1}{2} \sum_{\alpha\beta\gamma\delta} c_\alpha^\dagger c_\beta^\dagger c_\gamma c_\delta \langle \alpha\beta | \frac{1}{r_{12}} | \gamma\delta \rangle, \quad (17)$$

where c_γ is the annihilation operator of the one-electron spin-orbital wavefunction $|\gamma\rangle$ and c_α^\dagger is the creation operator of the one-electron spin-orbital wavefunction $|\alpha\rangle$. Then, the matrix element takes the form

$$\langle \Psi_{\text{fin}} | H_I^{\text{ee}} | \Psi_{\text{init}} \rangle_{\text{Auger}} = \frac{1}{2} \sum_{\alpha\beta\gamma\delta} \langle \Psi_{\text{fin}} | c_\alpha^\dagger c_\beta^\dagger c_\gamma c_\delta | \Psi_{\text{init}} \rangle \langle \alpha\beta | \frac{1}{r_{12}} | \gamma\delta \rangle. \quad (18)$$

Using the anti-commutation relations of the creation and annihilation operators, eqn (18) is written as

$$\langle \Psi_{\text{fin}} | H_I^{\text{ee}} | \Psi_{\text{init}} \rangle_{\text{Auger}} = \langle \zeta s | \frac{1}{r_{12}} | ba \rangle - \langle \zeta s | \frac{1}{r_{12}} | ab \rangle. \quad (19)$$

In the Auger transition matrix element, a and b are the one-electron wavefunctions of the two valence electrons, while s and ζ are the one-electron wavefunctions of the core and continuum electrons, respectively. In this transition, the core hole in spin-orbital s is filled by an electron from spin-orbitals a or b, while the other valence electron ionizes. Changing from the $m_a \mu_a m_b \mu_b$ to the $m_a m_b S M_S$ scheme we obtain

$$\mathcal{M} = \langle \Psi_{\text{fin}} | H_I^{\text{ee}} | \Psi_{\text{init}} \rangle_{\text{Auger}} = \delta_{S',S} \delta_{M'_S, M_S} \left(\langle \zeta s | \frac{1}{r_{12}} | ba \rangle + (-1)^S \langle \zeta s | \frac{1}{r_{12}} | ab \rangle \right). \quad (20)$$

m_a and μ_a are the projection of the orbital angular momentum and spin, respectively, while S is the total spin and M_S is the projection of the total spin. $\langle \zeta s | \frac{1}{r_{12}} | ba \rangle$ is the spatial part of the matrix element $\langle \zeta s | \frac{1}{r_{12}} | ba \rangle$ which is given by

$$\langle \zeta s | \frac{1}{r_{12}} | ba \rangle = \int d\mathbf{r} \phi_\zeta^* \phi_s^* \frac{1}{r_{12}} \phi_b \phi_a. \quad (21)$$

Using eqn (19) and eqn (21) and expressing the orbital wavefunctions in the SCE scheme, we find

$$\mathcal{M} = \delta_{S,S'} \delta_{M'_S, M'_S} \quad (22)$$

$$\times \left(\sum_{\substack{kl\zeta l_s, q=-k \\ l_b l_a}}^k \int d\mathbf{r}_1 \int d\mathbf{r}_2 P_{l_\zeta m_\zeta}^{\zeta*}(r_1) P_{l_s m_s}^{S*}(r_2) \frac{r_{12}^k}{r_{12}^{k+1}} P_{l_b m_b}^b(r_1) P_{l_a m_a}^a(r_2) \right.$$

$$\times (-1)^{m_s} \sqrt{(2l_s+1)(2l_a+1)} \begin{pmatrix} l_s & k & l_a \\ 0 & 0 & 0 \end{pmatrix} \begin{pmatrix} l_s & k & l_a \\ -m_s & q & m_a \end{pmatrix}$$

$$\times (-1)^{q+m_\zeta} \sqrt{(2l_\zeta+1)(2l_b+1)} \begin{pmatrix} k & l_\zeta & l_b \\ 0 & 0 & 0 \end{pmatrix} \begin{pmatrix} k & l_\zeta & l_b \\ -q & -m_\zeta & m_b \end{pmatrix}$$

$$\left. + (-1)^S \sum_{\substack{kl\zeta l_s, q=-k \\ l_b l_a}}^k \int d\mathbf{r}_1 \int d\mathbf{r}_2 P_{l_\zeta m_\zeta}^{\zeta*}(r_1) P_{l_s m_s}^{S*}(r_2) \frac{r_{12}^k}{r_{12}^{k+1}} P_{l_a m_a}^a(r_1) P_{l_b m_b}^b(r_2) \right.$$

$$\times (-1)^{m_s} \sqrt{(2l_s+1)(2l_b+1)} \begin{pmatrix} l_s & k & l_b \\ 0 & 0 & 0 \end{pmatrix} \begin{pmatrix} l_s & k & l_b \\ -m_s & q & m_b \end{pmatrix}$$

$$\left. \times (-1)^{q+m_\zeta} \sqrt{(2l_\zeta+1)(2l_a+1)} \begin{pmatrix} k & l_\zeta & l_a \\ 0 & 0 & 0 \end{pmatrix} \begin{pmatrix} k & l_\zeta & l_a \\ -q & -m_\zeta & m_a \end{pmatrix} \right)$$

Final State	Valence 1	Valence 2	This Work	Ref. 35
$^3\Sigma_u^+$	$2\sigma_u$	$3\sigma_g$	0.01	0.01
$^1\Sigma_u^+$	$2\sigma_u$	$3\sigma_g$	0.05	0.11
$^3\Pi_u$	$3\sigma_g$	$1\pi_{ux}(1\pi_{uy})$	0.01	0.01
$^1\Pi_u$	$3\sigma_g$	$1\pi_{ux}(1\pi_{uy})$	0.11	0.13
$^3\Pi_g$	$2\sigma_u$	$1\pi_{ux}(1\pi_{uy})$	0.02	0.03
$^1\Pi_g$	$2\sigma_u$	$1\pi_{ux}(1\pi_{uy})$	0.08	0.13
$^3\Pi_u$	$2\sigma_g$	$1\pi_{ux}(1\pi_{uy})$	0.03	0.01
$^1\Pi_u$	$2\sigma_g$	$1\pi_{ux}(1\pi_{uy})$	0.09	0.06
$^3\Sigma_u^+$	$2\sigma_g$	$2\sigma_u$	0.01	0.01
$^1\Sigma_u^+$	$2\sigma_g$	$2\sigma_u$	0.20	0.11
$^3\Sigma_g^+$	$2\sigma_g$	$3\sigma_g$	0.02	0.02
$^1\Sigma_g^+$	$2\sigma_g$	$3\sigma_g$	0.08	0.07
$^1\Sigma_g^+$	$3\sigma_g$	$3\sigma_g$	0.05	0.04
$^1\Delta_g$	$1\pi_{ux}(1\pi_{uy})$	$1\pi_{ux}(1\pi_{uy})$	0.09	0.12
$^1\Sigma_g^+$	$1\pi_{ux}(1\pi_{uy})$	$1\pi_{uy}(1\pi_{ux})$	0.03	0.01
$^1\Sigma_g^+$	$2\sigma_u$	$2\sigma_u$	0.05	0.13
$^1\Sigma_g^+$	$2\sigma_g$	$2\sigma_g$	0.07	0.02

Table 2 Ratio of each Auger transition for a 1s core-hole divided by the sum of all Auger transitions for a 1s core-hole for N_2

where $r_< = \min(r, r')$ and $r_> = \max(r, r')$. The Auger rate is given by

$$\Gamma_{b,a \rightarrow s, \zeta} = \sum_{\substack{m_a m_b m_s m_\zeta \\ S M_S S' M_S'}} \pi N_{12} N_h \sum_L |\mathcal{M}|^2, \quad (23)$$

with N_h the number of holes in the orbital to be filled. N_{12} is the weighting occupation factor given by

$$N_{12} = \begin{cases} \frac{N_{v1} N_{v2}}{2 \times 2} & \text{for different orbitals} \\ \frac{N_{v1} (N_{v1} - 1)}{2 \times 2 \times 1} & \text{for same orbital} \end{cases} \quad (24)$$

where N_{v1} and N_{v2} are the occupations numbers of the valence orbitals that are involved in the Auger transition. Next, we compare our results for the Auger rates of N_2^+ with a 1s core-hole, which are computed using eqn (23) with the Auger rates calculated using a Green's function method.³⁵ The 1s state corresponds to $\phi_{1s} = \frac{1}{\sqrt{2}} (\phi_{1\sigma_g} + \phi_{1\sigma_u})$. Using the orthogonality of the molecular states, it follows that the 1s Auger rates are obtained by averaging the Auger rates of the $1\sigma_g$ and $1\sigma_u$ core hole molecular states. In the work in ref. 35, only relative values of the Auger rates are given. Specifically, the ratio of each Auger rate with respect to the transition is given. To compare the results in ref. 35 with our values we divide each Auger transition by the sum of all Auger transitions for a 1s core-hole state. The resulting values are shown in Table 2 and the agreement is shown to be good. Moreover, we find that the sum of all Auger rates corresponding to a 1s core-hole is equal to $2.87E - 3$ a.u.. This value compares well with the experimental value of $3.77E - 3$ a.u. obtained in ref. 20. We note that the Auger rates we use to solve the rate equations are summed over all allowed spin configurations. The reason for this is that spin is not specified in the electronic configurations of the molecular states.

3 Results

Using the methods described in the previous sections, we compute the photo-ionization cross sections and the Auger transitions for all allowed molecular transitions up to N_2^{4+} for 525 eV and 1100

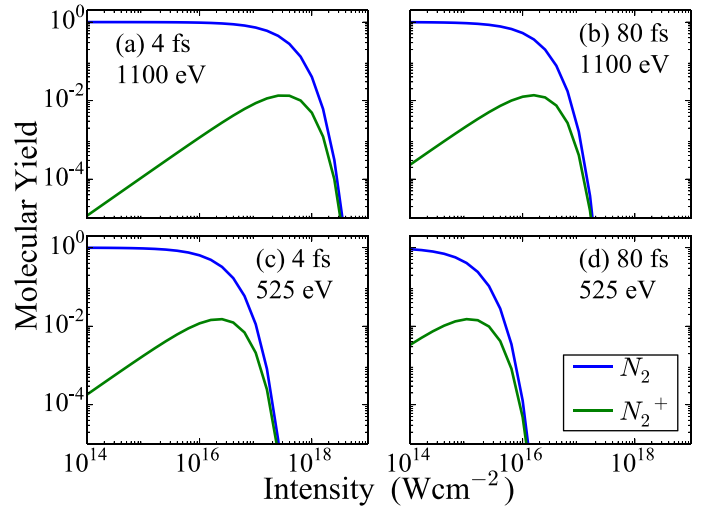


Fig. 2 Molecular ion yields resulting from the interaction of N_2 with four FEL pulses as a function of the intensity of the laser pulse

eV FEL pulses. N_2^{4+} is the highest molecular ion state that can be reached, since we assume that the N_2^{4+} state dissociates instantaneously. In addition, using the method we developed in ref. 10 we compute the Auger rates for all allowed atomic transitions while we obtain the atomic cross sections from ref. 36. We solve 309 rate equations to obtain the ion yields and the electron spectra. In addition, in order to obtain the population of all accessible pathways, we solve roughly 1.8×10^6 rate equations for the 525 eV FEL pulse and 6.6×10^6 rate equations for the 1100 eV FEL pulse. The computation of the pathway population allows us to identify the percentage of the contribution of SCH versus DCH molecular states to the final atomic ion yields.

3.1 Ion Yields

First, we compute the molecular and atomic ion yields for a 525 eV and 1100 eV FEL pulses. For each photon energy we consider two different full width half maximum (FWHM) durations of the FEL pulse, namely 4 fs and 80 fs. In Fig. 2, we show the dependence on intensity of the molecular ion yields resulting from the interaction of N_2 with four different FEL pulses. We find that only the N_2 and N_2^+ states are populated a long time after the end of the FEL pulses. This is expected, since, in our model, all higher charged states eventually dissociate. We also find that after a certain intensity the population of both the N_2 and the N_2^+ molecular states reduces significantly for all four FEL pulses considered. For the same photon energy FEL pulses, N_2 and N_2^+ are depleted at a smaller intensity for the 80 fs FEL-pulse compared to the 4 fs one. Comparing the molecular ion yields of FEL pulses with the same FWHM but different photon energy, we find that depletion of N_2 and N_2^+ occurs at a smaller intensity for the 525 eV FEL pulse. The reason for this is that the single-photon ionization cross sections for the molecular transitions, are larger for the 525 eV FEL pulse compared to the 1100 eV FEL pulse, for a certain intensity.

Next, in Fig. 3 we show the atomic ion yields for the same four FEL pulses as in Fig. 2 as a function of the laser intensity. Comparing the atomic ion yields of FEL pulses with the same photon

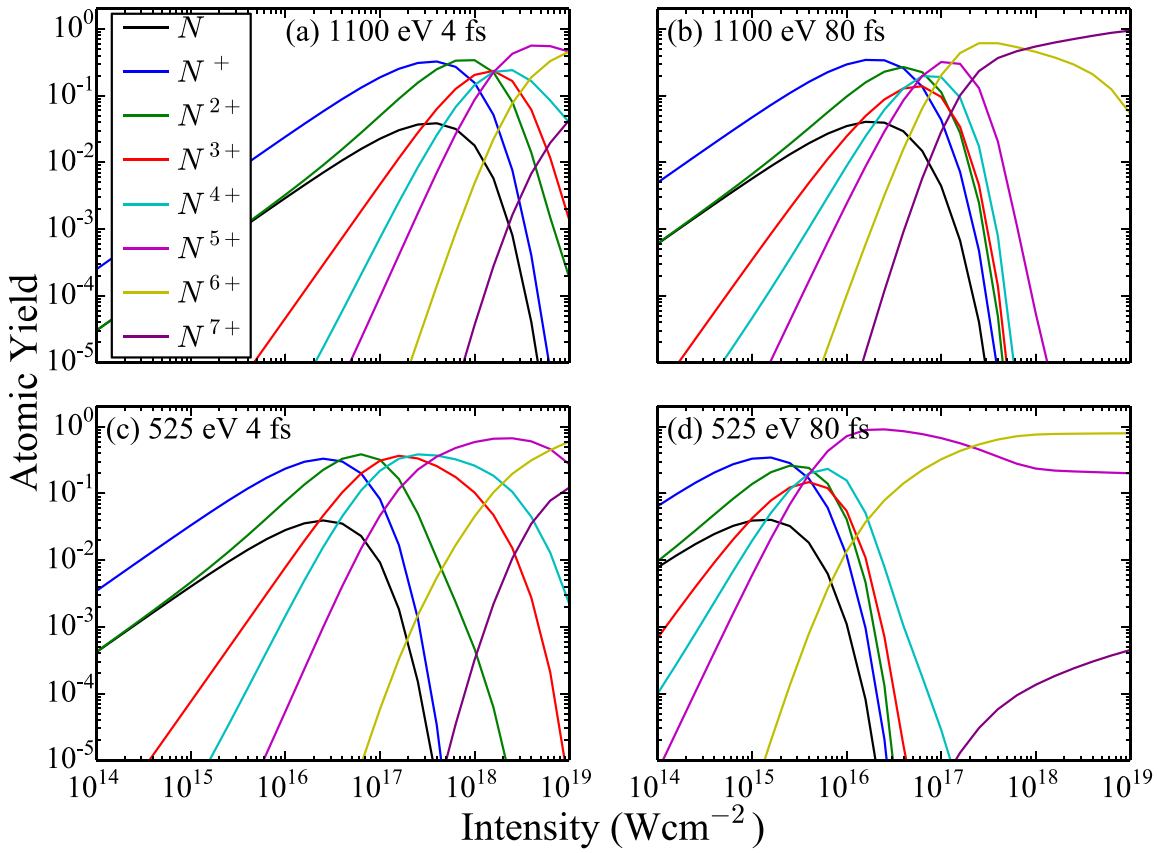


Fig. 3 Atomic ion yields resulting from the interaction of N_2 with four FEL pulses as a function of the intensity of the laser pulse

energy but different FWHM, we find that the population of the higher charged states becomes significant at smaller intensities for the 80 fs FEL pulse compared to the 4 fs one. This is expected, since more single-photon ionization processes take place during the longer FEL pulse. Next, we compare the atomic ion yields of FEL pulses with the same FWHM but different photon energy. We find that the population of the higher charged states becomes significant at smaller intensities for the 525 eV FEL pulse compared to the 1100 eV one. The reason for this is that the single-photon ionization cross sections both for the atomic and the molecular transitions are higher for the 525 eV FEL pulse.

3.2 Single versus Double Core Holes

We now compute all energetically accessible pathways that start from the N_2 ground state and end at ion fragments up to N^{7+} for a 4 fs FEL pulse. We identify the contribution to the atomic ion yields of pathways that have accessed only a SCH molecular state versus pathways that have accessed a DCH molecular state. This contribution is shown in Fig. 4 for a 525 eV and a 1100 eV FEL pulse at different laser pulse intensities.

First, we compare the results for two FEL pulses that have the same intensity of 10^{17} Wcm^{-2} but different photon energy, see Fig. 4 (a) and (c). We find that the population of the higher charged atomic ion states is much larger for the 525 eV FEL pulse. The reason for this is that the molecular and atomic photo-ionization cross sections as well as the photon flux are larger for the 525 eV

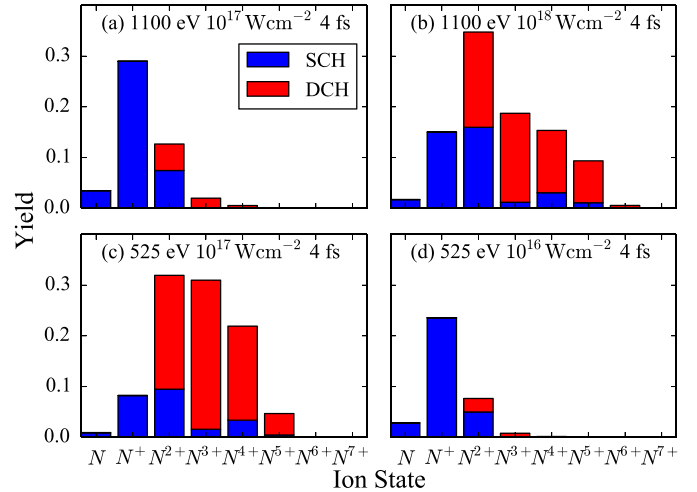


Fig. 4 Atomic ion yields and contribution of SCH and DCH molecular states for FEL pulses with 4 fs FWHM and photon energy of 525 eV and of 1100 eV

FEL pulse. Another consequence of the larger molecular photo-ionization cross sections is that for the 525 eV FEL pulse it is more probable for a second core hole to be created by single-photon ionization before an Auger transition takes place. This explains why the DCH molecular states contribute significantly more than the SCH molecular states to the population of the higher charged atomic ions, see Fig. 4(c). However, if a smaller intensity of 10^{16} Wcm $^{-2}$ is considered for the 525 eV FEL pulse, see Fig. 4(d), then similar results are obtained as for the 1100 eV FEL pulse at an intensity of 10^{17} Wcm $^{-2}$, see Fig. 4(a). In Fig. 4(b), it is shown that when a higher intensity of 10^{18} Wcm $^{-2}$ is considered for the 1100 eV FEL pulse, similar results are obtained as for the 525 eV FEL at a smaller intensity, see Fig. 4(c). That is, higher charged atomic ion states are significantly populated and the DCH molecular states contribute significantly to these yields. The reason for this is that the higher intensity counteracts the effects from the single-photon ionization cross sections being smaller for the 1100 eV FEL pulse compared to the 525 eV FEL pulse.

3.3 Electron spectra

Using the molecular and atomic Auger and photo-ionization yields, we plot the probability for an electron to ionize with a certain energy, that is, we plot the electron spectra in Fig. 5. Specifically, we plot the electron spectra for 525 eV and 1100 eV FEL pulses. For each photon energy two FWHM laser pulses are considered, namely of 4 fs and of 80 fs. Comparing the electron spectra corresponding to the same FWHM FEL pulse, i.e. Fig. 5 (a) with (c) and Fig. 5 (b) with (d), we find that there is a higher contribution of atomic transitions to the electron spectra for the 525 eV FEL pulse. As previously mentioned, the reason is that the molecular photo-ionization cross sections are larger for the smaller photon energy resulting in a larger population reaching higher charged molecular states which in turn dissociate into atomic ion fragments. The atomic photo-ionization cross sections are also higher for the 525 eV FEL pulse and so higher charged atomic ion states are thus reached. Moreover, comparing the electron spectra corresponding to the same photon energy FEL pulse, i.e. Fig. 5 (a) with (b) and Fig. 5 (c) with (d) we find that there is a higher contribution of atomic transitions to the electron spectra for the longer duration, 80 fs, FEL pulse. The longer pulse duration allows for a larger number of photo-ionization processes to take place which in turn leads to the production of more higher charged atomic ion states. We also note that for the 525 eV FEL pulse the electrons can escape with small energies. Thus, it is important that in our formulation the Auger and the photo-ionization rates are computed using molecular and not atomic continuum orbitals.

Finally, we investigate whether studying electron spectra is an efficient way of detecting the formation of DCH molecular states. To answer this question we plot the contribution to the Auger and photo-ionization yields of DCH molecular states. We find that the contribution to the electron spectra of DCH Auger molecular transitions is difficult to distinguish and overlaps with Auger atomic transitions. However, the DCH single-photon ionization molecular transitions are easier to distinguish. For instance there is a clear peak in the electron spectra due to DCH single-photon ionization

molecular transitions at around 55 eV for the case of the 525 eV 4 fs FEL pulse. This result suggests that photoionization electron spectra maybe a viable route for the detection of DCH molecular transitions.

4 Conclusions

We investigate the interaction of molecular nitrogen with FEL radiation. We computed molecular continuum orbitals in the single center expansion scheme and used these orbitals to compute the Auger rates and photo-ionization cross-sections for molecular nitrogen. Formulating rate equations for all energetically accessible molecular and atomic transitions, we investigated the dependence of the final fragments yields on the parameters of the FEL pulse. Moreover, we studied the contribution of the DCH molecular states to the final atomic ion yields. We found that for a relatively small photon energy of 525 eV, with 420 eV being the photon energy needed to create a core hole, already at intermediate intensities, DCH molecular states contribute significantly to the formation of the final atomic ion fragments. For a higher photon energy of 1100 eV FEL pulse, we find that a much higher intensity is needed in order for the DCH molecular states to significantly contribute to the final atomic ion fragments. Finally, we computed the contribution of the Auger and the single-photon ionization processes in the electron spectra. Our results suggest that single-photon ionization processes are a more efficient tool for detecting the formation of DCH molecular states in the electron spectra. Additional studies are needed to verify this and to investigate the effect of nuclear motion.

Acknowledgements

A. E. is grateful to Peter Lambropoulos for pointing out DCH formation as an interesting problem in molecules interacting with FEL pulses. A.E. acknowledges the use of the Legion computational resources at UCL.

A Direct and Exchange Coefficients

In the Hartree-Fock framework, after applying the variational principle,²⁸ the electron-electron interaction terms can be written as

$$\sum_i^{\text{orbs}} a_i J_i \phi_\epsilon - \sum_i^{\text{orbs}} b_i K_i \phi_\epsilon = \epsilon^{\text{ee}} \phi_\epsilon, \quad (25)$$

where ϕ_ϵ is the spin-orbital of the molecular continuum electron with spin orientation μ_ϵ and ϵ^{ee} is the energy contribution of the electron-electron interaction terms. The index i refers to a bound molecular orbital and J_i and K_i are defined as

$$J_i \phi_\epsilon = \langle \phi_i | \frac{1}{r_{12}} | \phi_i \rangle \phi_\epsilon \quad (26)$$

$$K_i \phi_\epsilon = \langle \phi_i | \frac{1}{r_{12}} | \phi_\epsilon \rangle \phi_i.$$

To obtain the a_i and b_i coefficients in the general case, it suffices to obtain a_i and b_i for three limiting cases. Since we consider molecular orbitals in all three limiting cases, the electron occupancy of the shells involved is zero, one or two. If a shell is not occupied, the coefficients a_i and b_i are zero. For the first limiting case, a

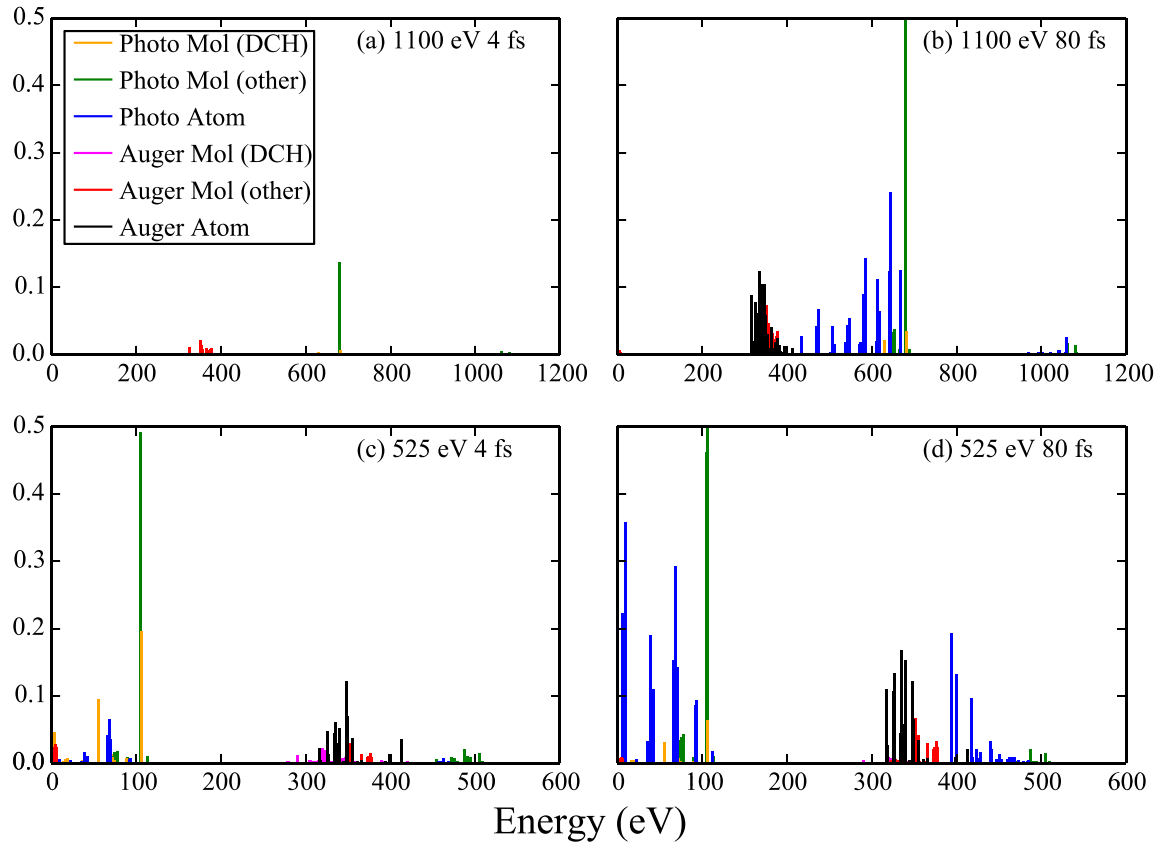


Fig. 5 Electron spectra resulting from the interaction of N_2 with FEL pulses at an intensity of $10^{17} \text{ W cm}^{-2}$

two-electron system is considered, with both electrons initially occupying a single shell i and one of these electrons finally being emitted to the continuum. Spin is conserved and it is equal to zero in the initial and final states. Therefore, a two-electron wavefunction must be constructed that is anti-symmetric in spin and anti-symmetric under exchange of electrons. Such a wavefunction is given as a sum of the following two Slater determinants

$$\Phi(q_1, q_2) = \frac{1}{\sqrt{2}} \left(\frac{1}{\sqrt{2!}} \begin{vmatrix} \phi_i^\uparrow(q_1) & \phi_\epsilon^\downarrow(q_1) \\ \phi_i^\uparrow(q_2) & \phi_\epsilon^\downarrow(q_2) \end{vmatrix} - \frac{1}{\sqrt{2!}} \begin{vmatrix} \phi_i^\downarrow(q_1) & \phi_\epsilon^\uparrow(q_1) \\ \phi_i^\downarrow(q_2) & \phi_\epsilon^\uparrow(q_2) \end{vmatrix} \right), \quad (27)$$

where q_1 and q_2 are the spin and space coordinates of the two electrons. Using spin conservation and exchange symmetry, it is found that the energy contribution of the electron-electron interaction term is given by

$$\epsilon^{\text{ee}} = \langle \Phi | \frac{1}{r_{12}} | \Phi \rangle = \langle \phi_i \phi_\epsilon | \frac{1}{r_{12}} | \phi_i \phi_\epsilon \rangle + \langle \phi_i \phi_\epsilon | \frac{1}{r_{12}} | \phi_\epsilon \phi_i \rangle. \quad (28)$$

Using the variational principle in the Hartree-Fock equations scheme²⁸ for the continuum orbital, the following equations are obtained

$$J_i \phi_\epsilon + K_i \phi_\epsilon = \epsilon^{\text{ee}} \phi_\epsilon. \quad (29)$$

Comparing eqn (25) and eqn (29), we find that $a_i = 1$ and $b_i = -1$.

Another limiting case involves two shells i and j . In the initial state one electron is in shell i and two electrons occupy shell j . In

the final state one electron from the j shell escapes to the continuum. A three-electron wavefunction must be constructed which is anti-symmetric in spin regarding the continuum electron and the electron in the j shell and anti-symmetric under exchange of electrons. Such a wavefunction is given as a sum of the following two Slater determinants

$$\Phi(q_1, q_2, q_3) = \frac{1}{\sqrt{2 \times 3!}} \begin{vmatrix} \phi_i^\uparrow(q_1) & \phi_j^\downarrow(q_1) & \phi_\epsilon^\uparrow(q_1) \\ \phi_i^\uparrow(q_2) & \phi_j^\downarrow(q_2) & \phi_\epsilon^\uparrow(q_2) \\ \phi_i^\uparrow(q_3) & \phi_j^\downarrow(q_3) & \phi_\epsilon^\uparrow(q_3) \end{vmatrix} - \frac{1}{\sqrt{2 \times 3!}} \begin{vmatrix} \phi_i^\uparrow(q_1) & \phi_j^\uparrow(q_1) & \phi_\epsilon^\downarrow(q_1) \\ \phi_i^\uparrow(q_2) & \phi_j^\uparrow(q_2) & \phi_\epsilon^\downarrow(q_2) \\ \phi_i^\uparrow(q_3) & \phi_j^\uparrow(q_3) & \phi_\epsilon^\downarrow(q_3) \end{vmatrix}. \quad (30)$$

Following the same procedure as for the other limiting case, the following equations are obtained

$$(J_i - \frac{1}{2}K_i + J_j + K_j) \phi_\epsilon = \epsilon^{\text{ee}} \phi_\epsilon, \quad (31)$$

Comparing eqn (25) and eqn (31), it is found that $a_j = 1$ and $b_j = -1$, while $a_i = 1$ and $b_i = \frac{1}{2}$.

The third limiting case involves two electrons occupying shell i and two electrons occupying shell j in the initial state, with one electron from orbital j escaping to the continuum in the final state. Following the same procedure as in the other two cases, it can be shown that $a_i = 2$ and $b_i = 1$ and $a_j = 1$ and $b_j = -1$. In general, for

all molecular ion states, in the Hartree-Fock formalism, the occupation coefficients a_i and b_i can be obtained using the above three limiting cases.

References

- 1 C. Pellegrini, *European Physical Journal H*, 2012, **37**, 659–708.
- 2 J. Marangos, *Contemporary Physics*, 2011, **52**, 551–569.
- 3 J. Ullrich, A. Rudenko and R. Moshhammer, *Annual Review of Physical Chemistry*, 2012, **63**, 635–660.
- 4 I. Schlichting and J. Miao, *Current Opinion in Structural Biology*, 2012, **22**, 613 – 626.
- 5 R. Neutze, R. Wouts, D. van der Spoel, E. Weckert and J. Hajdu, *Nature*, 2000, **406**, 752–757.
- 6 L. Redecke, K. Nass, D. P. DePonte, T. A. White, D. Rehders, A. Barty, F. Stellato, M. Liang, T. R. Barends, S. Boutet, G. J. Williams, M. Messerschmidt, M. M. Seibert, A. Aquila, D. Arnold, S. Bajt, T. Barth, M. J. Bogan, C. Caleman, T.-C. Chao, R. B. Doak, H. Fleckenstein, M. Frank, R. Fromme, L. Galli, I. Grotjohann, M. S. Hunter, L. C. Johansson, S. Kassemeyer, G. Katona, R. A. Kirian, R. Koopmann, C. Kupitz, L. Lomb, A. V. Martin, S. Mogk, R. Neutze, R. L. Shoeman, J. Steinbrener, N. Timneanu, D. Wang, U. Weierstall, N. A. Zatsepin, J. C. H. Spence, P. Fromme, I. Schlichting, M. Duszynski, C. Betzel and H. N. Chapman, *Science*, 2013, **339**, 227–230.
- 7 L. S. Cederbaum, F. Tarantelli, A. Sgamellotti and J. Schirmer, *The Journal of Chemical Physics*, 1986, **85**, 6513–6523.
- 8 M. Tashiro, M. Ehara, H. Fukuzawa, K. Ueda, C. Buth, N. V. Kryzhevoi and L. S. Cederbaum, *The Journal of Chemical Physics*, 2010, **132**, 184302.
- 9 H. Pulkkinen, S. Aksela, O.-P. Sairanen, A. Hiltunen and H. Aksela, *Journal of Physics B: Atomic, Molecular and Optical Physics*, 1996, **29**, 3033.
- 10 A. O. G. Wallis, H. I. B. Banks and A. Emmanouilidou, *Phys. Rev. A*, 2015, **91**, 063402.
- 11 P. Lablanquie, L. Andric, J. Palaudoux, U. Becker, M. Braune, J. Vieffhaus, J. Eland and F. Penent, *Journal of Electron Spectroscopy and Related Phenomena*, 2007, **156–158**, 51 – 57.
- 12 C. P. Bhalla, N. O. Folland and M. A. Hein, *Phys. Rev. A*, 1973, **8**, 649–657.
- 13 S.-K. Son and R. Santra, *Phys. Rev. A*, 2012, **85**, 063415.
- 14 M. G. Makris, P. Lambropoulos and A. Mihelič, *Phys. Rev. Lett.*, 2009, **102**, 033002.
- 15 C. Buth, J. P. Cryan, J. M. Glowonia, M. Hoener, R. N. Coffee and N. Berrah, *The Journal of Chemical Physics*, 2012, **136**, 214310.
- 16 J.-C. Liu, N. Berrah, L. S. Cederbaum, J. P. Cryan, J. M. Glowonia, K. J. Schafer and C. Buth, *Journal of Physics B: Atomic, Molecular and Optical Physics*, 2016, **49**, 075602.
- 17 Y. Hao, L. Inhester, K. Hanasaki, S.-K. Son and R. Santra, *Structural Dynamics*, 2015, **2**, 041707.
- 18 Z. Jurek, S.-K. Son, B. Ziaja and R. Santra, *Journal of Applied Crystallography*, 2016, **49**, 1048–1056.
- 19 L. Inhester, K. Hanasaki, Y. Hao, S.-K. Son and R. Santra, *Phys. Rev. A*, 2016, **94**, 023422.
- 20 L. Fang, M. Hoener, O. Gessner, F. Tarantelli, S. T. Pratt, O. Kornilov, C. Buth, M. Gühr, E. P. Kanter, C. Bostedt, J. D. Bozek, P. H. Bucksbaum, M. Chen, R. Coffee, J. Cryan, M. Glowonia, E. Kukkk, S. R. Leone and N. Berrah, *Phys. Rev. Lett.*, 2010, **105**, 083005.
- 21 J. P. Cryan, J. M. Glowonia, J. Andreasson, A. Belkacem, N. Berrah, C. I. Blaga, C. Bostedt, J. Bozek, N. A. Cherepkov, L. F. DiMauro, L. Fang, O. Gessner, M. Gãijhr, J. Hajdu, M. P. Hertlein, M. Hoener, O. Kornilov, J. P. Marangos, A. M. March, B. K. McFarland, H. Merdji, M. Messerschmidt, V. S. Petrovič, C. Raman, D. Ray, D. A. Reis, S. K. Semenov, M. Trigo, J. L. White, W. White, L. Young, P. H. Bucksbaum and R. N. Coffee, *Journal of Physics B: Atomic, Molecular and Optical Physics*, 2012, **45**, 055601.
- 22 K. Ueda, R. Püttner, N. A. Cherepkov, F. Gel'mukhanov and M. Ehara, *The European Physical Journal Special Topics*, 2009, **169**, 95–107.
- 23 H. J. Werner, P. J. Knowles, R. Lindh, F. R. Manby, M. Schütz *et al.*, *MOLPRO, a package of ab initio programs*, 2010, see <http://www.molpro.net/>.
- 24 C. Beylerian and C. Cornaggia, *Journal of Physics B: Atomic, Molecular and Optical Physics*, 2004, **37**, L259.
- 25 M. Coville and T. D. Thomas, *Phys. Rev. A*, 1991, **43**, 6053–6056.
- 26 N. Rohringer and R. Santra, *Phys. Rev. A*, 2007, **76**, 033416.
- 27 P. V. Demekhin, A. Ehresmann and V. L. Sukhorukov, *The Journal of Chemical Physics*, 2011, **134**, 024113.
- 28 B. Bransden and C. Joachain, *Physics of Atoms and Molecules*, Prentice-Hall, 2002.
- 29 Shore and Menzel, *Principles of Atomic Spectra*, Wiley, 1968.
- 30 J. J. Sakurai, *Modern Quantum Mechanics*, Addison-Wesley, 1994.
- 31 S. K. Semenov, N. A. Cherepkov, G. H. Fecher and G. Schön-hense, *Phys. Rev. A*, 2000, **61**, 032704.
- 32 W. Pauli, *Wave Mechanics: Volume 5 of Pauli Lectures on Physics*, Wiley, 2000, pp. 150–151.
- 33 R. Manne and H. Ågren, *Chemical Physics*, 1985, **93**, 201 – 208.
- 34 L. Inhester, *Ph.D. thesis*, Georg-August-Universität Göttingen, 2013.

- 35 C. M. Liegener, *Journal of Physics B: Atomic and Molecular Physics*, 1983, **16**, 4281. <http://aphysics2.lanl.gov/tempweb/lanl/>.
- 36 Los Alamos National Laboratory Atomic Physics Codes; see